Nonreciprocal transparency in asymmetric gyrotropic trimers

Jin Wang [1], Ya Jie Liu,[1] Hui Yuan Dong,[2] Zheng-Gao Dong [1], and Kin Hung Fung[3,*]
[1]*School of Physics, Southeast University, Nanjing 211189, China*
[2]*School of Science, Nanjing University of Posts and Telecommunications, Nanjing 210003, China*
[3]*Department of Applied Physics, The Hong Kong Polytechnic University, Hong Kong, China*

(Received 15 September 2021; accepted 8 February 2022; published 22 February 2022)

We demonstrate theoretically an extreme scattering nonreciprocity, namely nonreciprocal transparency, in an asymmetric aggregate of deep-subwavelength gyrotropic trimer rods. By examining the asymmetric characteristics indicated in the differential extinction efficiency spectra, we explicitly reveal the underlying mechanism of such pronounced scattering nonreciprocity, arising from the asymmetrical magnetoelectric cross interactions besides the simultaneous excitations of the rotating magnetic dipole and electric dipole at each rod. Further, both far-field and near-field distributions are also investigated to validate our finding through full-wave numerical simulations. It may shed new light on the field of optics and photonics related to the nonreciprocal scattering on particle clusters.

DOI: 10.1103/PhysRevResearch.4.013147

I. INTRODUCTION

Light scattering by subwavelength objects is of fundamental importance in various physical branches [1–5], such as optical communications, sensing, and noninvasive detections. Many interesting scattering phenomena of reciprocal photonic elements have been reported, for instance, scattering dark states [6–8], superscattering [9–11], superabsorption [12–15], and unidirectional scattering [16–20]. Recently, the study of scattering asymmetry has been focused on a class of non-Hermitian parity-time (PT) symmetrical structures with balanced loss and gain [21–27], exhibiting totally different reflection (or backward scattering) when light beams are incident from two opposite sides. Likewise, theoretical analysis [28,29] and experimental observations [30–32] of transmission asymmetry (or difference in forward scattering) are also demonstrated through planar chiral metamaterials for forward and backward incident circularly or linearly polarized light. However, the "unidirectional" or "one-way" reflection found in those PT-symmetric linear systems and "asymmetrical" transmission claimed in chiral structures does not break the Lorentz reciprocity and thus cannot support nonreciprocal transparency [33,34]. With the increasing demand for miniaturization of photonic elements, true Lorentz nonreciprocal scattering elements are among the most challenging.

Figure 1 schematically illustrates the scattering nonreciprocity by a finite number N of particles of arbitrary cross section, exhibiting unique asymmetrical characteristics in the forward scattering amplitude (or total extinction cross section) for light beams with the same polarization and opposite incident directions. In particular, scattering is invisible to the outside observer for incidence from the left side [Fig. 1(a)], while it is observable for incidence from the right side [Fig. 1(b)]. Such intriguing nonreciprocal scattering phenomena are crucially important in the theoretical research and practical applications of nonreciprocal elements (isolators, circulators, and etc.), stable laser devices, and integrated photonic circuits [35–39]. To achieve the nonreciprocity, one needs to break all related symmetries, including time-reversal symmetry, spatial inversion, mirror symmetry, and symmetries in material parameters. To date, several approaches have been proposed, including the use of magneto-optical materials [40–42], spatiotemporal modulation of system parameters [43,44], or nonlinearity [45,46].

In this work, we present an extreme scattering nonreciprocity in collections of deep-subwavelength gyrotropic trimer rods. Specifically, nonreciprocal transparency is possibly achieved under the light illumination from two particular opposite sides, as shown in Fig. 1. Based on a scattering matrix formalism, we calculate the total extinction and differential scattering cross section of the subwavelength rod clusters to verify this nonreciprocal effect. Furthermore, we analyze and discuss the respective contributions to the total extinction from all multipolar resonances supported at each rod. It is revealed explicitly that the asymmetrical magnetoelectric cross interaction, i.e., the coupling between the magnetic dipole (MD) and electric dipole (ED) excitations, plays a vital role in the scattering nonreciprocity. In comparison with previous theoretical analysis by means of mathematical presentation [34,47], one can here readily gain insight into the underlying physical mechanism on scattering nonreciprocity and further figure out the interplay between spectral nonreciprocity and broken spatiotemporal symmetries in subwavelength rod clusters.

*khfung@polyu.edu.hk

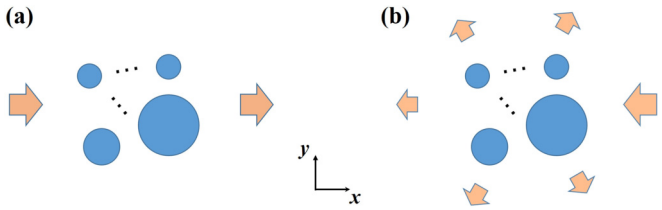

FIG. 1. Schematic illustration of scattering nonreciprocity for a set of finite-number N gyrotropic cylindrical rods. (a) The scattering is invisible to the outside observer for the incidence from the left side. (b) Strong scattering is observed for the incidence from the right side.

II. MODEL AND METHOD

Let us consider a two-dimensional scattering problem of subwavelength rod clusters in the x-y plane as represented in Fig. 2(a). The clusters consist of $N = 3$ infinitely long cylindrical gyromagnetic rods arranged along the z direction. The rods have different radii R_1, R_2, and R_3. For the sake of convenience, the rod centers are located on a circle of radius R, of which coordinate positions are denoted by $(x, y) = (R, 0), (-R/2, \pm\sqrt{3}R/2)$, respectively. The normally incident monochromatic plane wave has transverse electric (TE) polarization (electric field along the z direction), with its wave vector $\mathbf{k}$ having an angle α with respect to the x axis. In the presence of external static magnetic field H_0 along the z direction, the permeability tensor of the gyromagnetic material is

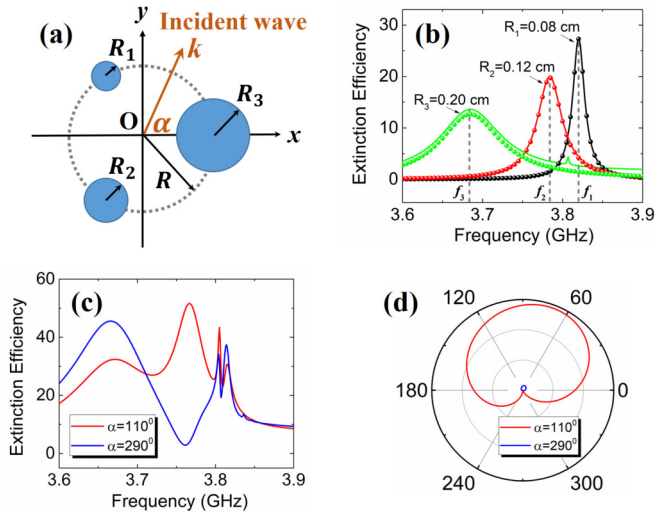

FIG. 2. (a) A two-dimensional scattering problem in the xy plane of the circular array composed of $N = 3$ gyromagnetic (YIG) cylindrical trimer rods under the normal illumination of external plane waves at an incident angle α with respect to the x direction. The geometrical parameter R is the radius of the array, and R_j $(j = 1, \ldots, 3)$ denotes the radius of an individual rod, respectively. (b) Extinction efficiency spectra for a single isolated rod with the radius $R_1 = 0.08\,\text{cm}$, $R_2 = 0.12\,\text{cm}$, and $R_3 = 0.20\,\text{cm}$. Here both the total extinction efficiency spectra (solid lines) and those spectra contributed only by the magnetic dipoles (black/red/green spheres) are shown. (c) Extinction efficiency spectra for the entire array structure with the incidence angles $\alpha = 110^\circ$ and 290°. (d) The distribution of differential scattering cross section at a frequency $f = 3.76\,\text{GHz}$ with the incidence angles $\alpha = 110^\circ$ and 290°.

given by [48,49]

$$\boldsymbol{\mu} = \begin{pmatrix} \mu_1 & i\mu_2 & 0 \\ -i\mu_2 & \mu_1 & 0 \\ 0 & 0 & 1 \end{pmatrix}, \tag{1}$$

with the elements $\mu_1 = 1 + \omega_m(\omega_h - i\eta\omega)/((\omega_h - i\eta\omega)^2 - \omega^2)$ and $\mu_2 = \omega_m\omega/((\omega_h - i\eta\omega)^2 - \omega^2)$, where $\omega_h = \gamma H_0$, $\omega_m = \gamma 4\pi M_s$, γ is the gyromagnetic ratio, η is the phenomenological damping coefficient, and $4\pi M_s$ denotes the saturation magnetization. Without loss of generality, we use here a type of commercially available gyromagnetic material, yttrium iron garnet (YIG), for the rods, with $H_0 = 500$ Oe, $4\pi M_s = 1750$ G, $\eta = 3 \times 10^{-4}$, and the permittivity $\epsilon_m = 15$. The background medium is set to be vacuum. Throughout this work, the $e^{-i\omega t}$ time-dependent convention for the harmonic field is used.

We start with the simplest scattering configuration of a single isolated gyromagnetic rod under normal illumination of incident plane waves. To see the electromagnetic response excited at each rod j $(j = 1, \ldots, N)$, we use the general Mie theory [1] to calculate the extinction efficiency,

$$Q_{\text{ext}}^{j} = \frac{2}{kR_j} \sum_{m=-\infty}^{\infty} \text{Re}[a_{j,m}] \tag{2}$$

where m is the cylindrical harmonic number, k is the angular wave number in the background, $\text{Re}[\cdot]$ denotes taking the real part, the radius R_j of the jth rod is chosen within deep-subwavelength size, i.e., $R_1 = 0.08\,\text{cm}$, $R_2 = 0.12\,\text{cm}$, and $R_3 = 0.20\,\text{cm}$, and $a_{j,m}$ is the complex scattering coefficient for the single rod j, given by [50]

$$a_{j,m} = \frac{\beta_j J_m(\delta_j) J_m'(\beta_j) - \zeta(\delta_j) J_m(\beta_j)}{\beta_j J_m(\delta_j) H_m'^{(1)}(\beta_j) - \zeta(\delta_j) H_m^{(1)}(\beta_j)}, \tag{3}$$

with $\zeta(\delta_j) = m\mu_k J_m(\delta_j) + \delta_j \mu_r J_m'(\delta_j)$. Here $\mu_r = \mu_1/(\mu_1^2 - \mu_2^2)$ and $\mu_k = -\mu_2/(\mu_1^2 - \mu_2^2)$. $J_m(\beta_j)$, $J_m(\delta_j)$, $H_m^{(1)}(\beta_j)$, and their primes respectively denote the mth-order Bessel and the first kind of Hankel functions and their corresponding derivatives with the arguments of $\beta_j = kR_j$ and $\delta_j = \beta_j\sqrt{\epsilon_m/\mu_r}$. Owing to the lack of time-reversal symmetry and reciprocity in the gyromagnetic materials, the scattering coefficients are generally asymmetric, $a_{j,m} \neq a_{j,-m}$. Relying on the direction (along z or $-z$ axis) of the applied magnetic field, only a series of cylindrical harmonic number m (negative or positive m) for the rotating magnetic multipoles can be supported [50].

The total extinction efficiency spectra and those contributed only by the magnetic dipoles ($m = -1$) are plotted in Fig. 2(b) by solid lines and black/red/green spheres, respectively. Apparently, the rotating MD resonances are dominant and excited at the respective frequencies $f_1 = 3.82\,\text{GHz}$, $f_2 = 3.78\,\text{GHz}$, and $f_3 = 3.68\,\text{GHz}$ for different rods. It is worth noting that, for the case of the rod with largest radius R_3, the total extinction spectra slightly shift up in comparison with the results under MD approximation, stemming from the non-negligible contribution from the ED excitation ($m = 0$). Additionally, the high-order magnetic quadrupole (MQ) resonance ($m = -2$) is also seen around a frequency $f = 3.8\,\text{GHz}$.

We now turn to the scattering case of collections of N parallel gyromagnetic rods shown in Fig. 2(a). Based on a

scattering matrix approach [51–53], the total incident field toward the jth rod contains two components: the total incident field of the external plane wave and the field scattered by all the other rods toward the jth rod, and we can obtain the relation between the multirod scattering coefficient $b_{j,m}$ and the single-rod scattering coefficient $a_{j,m}$ for the jth rod in a local system of cylindrical coordinates (with the origin located at the center of the jth rod):

$$b_{j,m} = a_{j,m}P_{j,m} + \sum_{l\neq j}^{l=1:N}\sum_{q=-\infty}^{\infty} a_{j,m}C_{j,l,m,q}b_{l,q}. \tag{4}$$

Here $P_{j,m}$ is the Fourier-Bessel expansion coefficient of the incident plane wave link to the jth rod with the polar coordinate of its center (r_j, θ_j) in the general xy system, $P_{j,m} = (-1)^m \exp[ikr_j \sin(\alpha - \theta_j) - im\alpha]$, and $C_{j,l,m,q}$ is the coupling matrix components that represent the coupling strength between the mth cylindrical harmonic of the jth rod and the qth cylindrical harmonic of the lth rod, given by $C_{j,l,m,q} = \exp[i(q-m)\theta_j^l]H_{m-q}^{(1)}(kr_j^l)$. Here, $H^{(1)}(\cdot)$ is the Hankel function of the first kind, and r_j^l and θ_j^l respectively show the relative distance and relative polar angle between the jth and lth rod centers.

Under the coordinate transformation from the local system to general xy system by applying Graf's formula [54], the scattering coefficient for the entire set of rods reads

$$b_q = \sum_{j=1}^{N}\sum_{m=-\infty}^{\infty} b_{j,m}e^{i(m-q)\theta_j}J_{q-m}(kr_j), \tag{5}$$

with $J(\cdot)$ being the Bessel function. By using the asymptotic form of the scattering field at infinity, we finally get the angular distribution $g(\theta)$ of scattering fields,

$$g(\theta) = \sqrt{\frac{2}{\pi k}}e^{-i\pi/4}\sum_{q=-\infty}^{\infty} b_q e^{iq(\theta-\pi/2)}, \tag{6}$$

and further the extinction efficiency Q_{ext}^a for the whole system according to the optical theorem [1],

$$Q_{\text{ext}}^a = -\frac{1}{R_1}\sqrt{\frac{2\pi}{k}}\,\text{Re}[e^{i\pi/4}g(\alpha+\pi)], \tag{7}$$

where α is the incident angle of external plane waves, as marked in Fig. 2(a). Note that here for convenience the extinction efficiency is defined as the total extinction cross section divided by the diameter of the first rod, $2R_1$.

III. RESULTS

By taking two particular incident directions from opposite sides, i.e., $\alpha = 110^\circ$ and 290°, we then show in Fig. 2(c) the total extinction efficiency spectra Q_{ext}^a for a set of cylindrical gyromagnetic rods $N = 3$, where the geometrical parameters are set as $R = 0.4$ cm, $R_1 = 0.08$ cm, $R_2 = 0.12$ cm, and $R_3 = 0.20$ cm. Remarkably, strong asymmetry in the extinction is observable over a broad frequency range before 3.80 GHz. In particular, at a frequency $f = 3.76$ GHz, enhanced scattering is seen under light illumination with incident angle $\alpha = 110^\circ$ [Fig. 2(c), the red line], whereas very weak scattering with nearly zero extinction appears for the opposite incidence $\alpha = 290^\circ$ [Fig. 2(c), the blue line]. The differential scattering cross section $D(\theta)$ in Fig. 2(d), defined as $D(\theta) = 2\pi|g(\theta)|^2$, also indicates unambiguously very strong nonreciprocity from these two scattering configurations. Notice that the frequency point where the most pronounced scattering asymmetry occurs lies in the off-resonance state of individual rods, implying that the cooperative effect of multiple resonances discussed below may be of crucial importance to the scattering nonreciprocity.

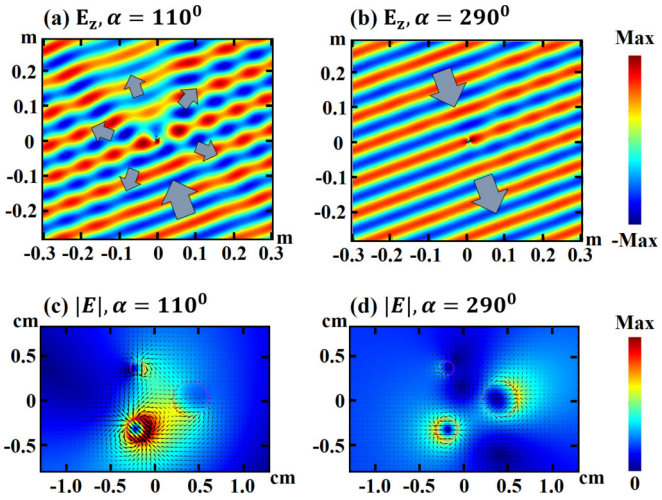

FIG. 3. Total field distribution around the proposed entire structure in Fig. 2(a), when the external plane wave is illuminated at a frequency $f = 3.76$ GHz, with an incident angle (a),(c) $\alpha = 110^\circ$ and (b),(d) $\alpha = 290^\circ$, respectively. (a),(b) The electric field E_z over the whole scattering space. (c),(d) Near-field distribution of the norm of electric field $|E|$ in the contour plot and the magnetic field $\mathbf{H} = (H_x, H_y)$ in the surface arrow plot. Note that the big gray arrows in (a),(b) are inserted manually, as guidance for readers to see the wave propagation.

This significant nonreciprocal effect can be readily visualized using full-wave simulations based on a finite element solver (COMSOL MULTIPHYSICS). Figure 3 depicts the total spatial field distribution around the proposed assembly of gyromagnetic rods, under the illumination of an external plane wave at a frequency of $f = 3.76$ GHz, with incident angles $\alpha = 110^\circ$ [Figs. 3(a) and 3(c)] and $\alpha = 290^\circ$ [Figs. 3(b) and 3(d)]. For the case of upward incidence shown in Fig. 3(a), the wave profile in the forward direction is distorted seriously, and a large "shadow" is observed, whose size is much larger than the structure dimension. We further zoom in and get a closeup view of magnetic field distribution $\mathbf{H} = (H_x, H_y)$ with black arrows shown in Fig. 3(c). It is observed that strong resonances are excited simultaneously at individual rods, particularly the MD resonance at the first and second rods. Besides, the strong cooperative effect among different rods is clearly visible. All these combined effects lead to the significant scattering. In contrast, for downward incidence in Fig. 3(b), the scattering is almost invisible to the outside observer, resulted from the strong suppression of the resonances at rods as well as the coupling interactions shown in Fig. 3(d). As a consequence, for collections of subwavelength

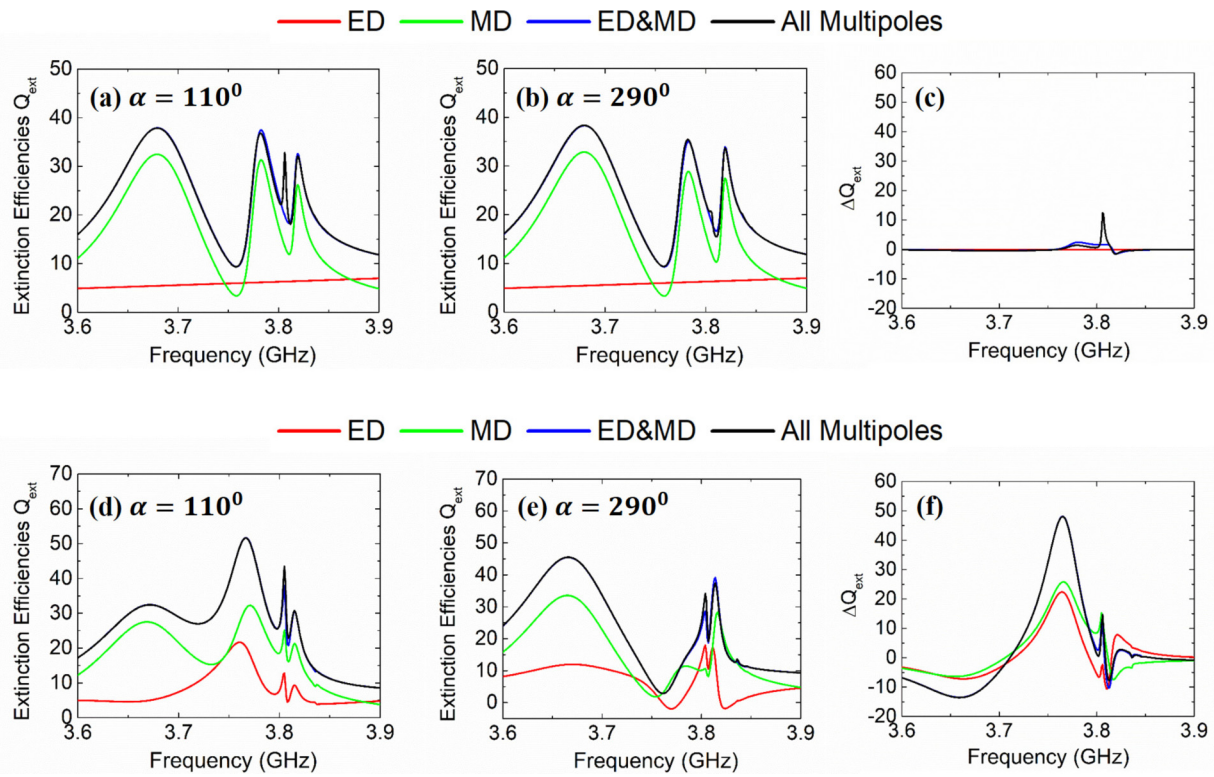

FIG. 4. Extinction efficiency spectra (a),(b) and (d),(e), and scattering nonreciprocity (c),(f) for the proposed entire structure when the magnetoelectric cross interaction among the rods is neglected (a)–(c) and considered (d)–(f). Total extinction and the individual contributions from ED, MD, and dual dipole (ED&MD) are shown at incident angles $\alpha = 110^\circ$ (a),(d) and $\alpha = 290^\circ$ (b),(e), respectively.

gyromagnetic rods, nonreciprocal transparency is attained in this case.

To further clarify the underlying mechanisms associated with the unidirectional nonreciprocal transparency identified above in Fig. 3, we separate analytically different contributions from the ED ($a_{j,m} = 0$ when $m \neq 0$), MD ($a_{j,m} = 0$ when $|m| \neq 1$), and ED&MD ($a_{j,m} = 0$ when $|m| > 1$) to all multipoles in the total extinction, when the magnetoelectric cross coupling (the coupling between ED and magnetic multipoles) is absent [Figs. 4(a)–4(c)] or present [Figs. 4(d)–4(f)]. Through setting the coupling matrix $C_{j,l,m,q} = 0$ in Eq. (4) when $m \neq q$ and $m \cdot q = 0$, we neglect the magnetoelectric cross coupling to calculate the extinction efficiencies shown in Figs. 4(a)–4(c). In comparison with the two scattering cases of upward or downward incidence in Fig. 3, the dominant MD and broad ED resonances are supported at identical frequencies, which are both independent of the incident angle of external plane waves. The exception is that, only for the upward incidence ($\alpha = 110^\circ$), there exists an additional scattering peak around 3.8 GHz, corresponding to the excitation of MQ resonance. As a result, by examining the difference in total extinction efficiencies $\Delta Q_{\text{ext}} (= Q_{\text{ext}}|_{\alpha=110^\circ} - Q_{\text{ext}}|_{\alpha=290^\circ})$, the scattering is totally reciprocal with zero ΔQ_{ext} under the approximation of no magnetoelectric cross coupling, but with an only exception when the high-order magnetic multipole, i.e., MQ resonance, is excited asymmetrically.

In contrast, by taking into consideration the magnetoelectric cross coupling, the contributions to the total extinction from purely ED, purely MD, and ED&MD shows in Figs. 4(d)–4(f) significant difference between upward ($\alpha = 110^\circ$) and downward ($\alpha = 290^\circ$) incidence. To be more specific, unidirectional nonreciprocal transparency occurs around a frequency $f = 3.76$ GHz, accompanied by the presence of very large extinction for upward incidence, and almost zero extinction for downward incidence. To sum up, the formation of the scattering nonreciprocity here basically comes from a class of asymmetrical modal interference, magnetoelectric cross interactions, besides the simultaneous excitations of ED and MD at individual rods. As an analogy, Wang *et al.* [42] recently demonstrated Maxwell's demon-like nonreciprocity in a class of non-Hermitian gyrotropic metasurfaces, explained by the asymmetrical absorption in lossy dielectric cylinders under the cooperative effect of the rotating MD and ED excited in the metasurface. The underlying mechanisms in these two examples are substantially identical, revealing explicitly that the asymmetry in the magnetoelectric cross interaction plays a vital role on the nonreciprocity for the infinite periodic or finite-number scattering systems.

Instead of the specified opposite illumination at the above example, we proceed to investigate in Fig. 5 the influence of other incident directions to the scattering nonreciprocity over the frequency range of interest. By considering the all multipolar excitations and also the magnetoelectric cross coupling in Fig. 5(a), the extinction efficiency spectra show unique nonreciprocal properties before 3.8 GHz for the case of incident angle $\alpha \in [0^\circ, 180^\circ]$, compared to that of $\alpha \in [180^\circ, 360^\circ]$. On the other hand, except for the asymmetric excitation of MQ resonance at a narrow frequency region around 3.8 GHz, the extinctions Q_{ext} in Fig. 5(a) are in good agreement with

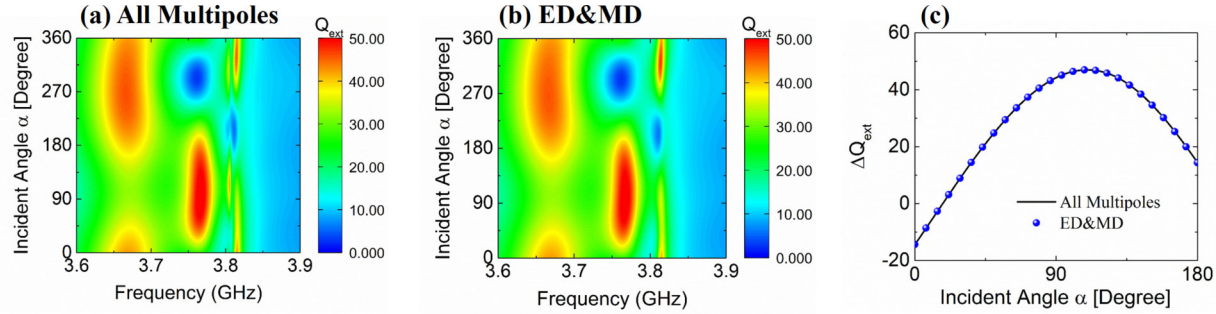

FIG. 5. The relation between the incident angle α and extinction efficiencies spectra from the contributions of (a) all multipoles and (b) dual dipole (ED&MD). (c) The comparison of difference in extinction efficiencies spectra for different incident angles at a frequency $f = 3.76\,\mathrm{GHz}$ under the consideration of total multipoles and dual-dipole (ED&MD) approximation.

those in Fig. 5(b) under the dual-dipole (MD&ED) approximation ($a_{j,m} = 0$ when $|m| > 1$). As an example in Fig. 5(c), the nonreciprocity ΔQ_{ext} at the frequency $f = 3.76\,\mathrm{GHz}$ is totally identical between them for different external incidence, showing in this case the validity of the dual-dipole model for the demonstration of the scattering problem for a finite number of deep-subwavelength gyromagnetic rods, where these rods are not too close together.

We finally clarify the impact of the geometrical parameters in the system on the scattering nonreciprocity. For example, we tune the radius R of the circle shown in Fig. 2(a) and keep the individual rod centers located at the circle, simultaneously with their polar angles unchanged in the general xy system. In Fig. 6, we depict the extinction efficiency spectra Q_{ext} and the nonreciprocity ΔQ_{ext} as a function of R for opposite illuminations $\alpha = 110^\circ$ and 290°. The extinction at the incident angle $\alpha = 110^\circ$ shown in Fig. 6(a) remains strong around $f = 3.76\,\mathrm{GHz}$ but with slow reduction as R increases, whereas that at $\alpha = 290^\circ$ indicated in Fig. 6(b) at the same frequency remains inconspicuous. It is thereby shown in Fig. 6(c), that the significant nonreciprocity can be maintained well over a broad system of a finite number of gyromagnetic rods. However, by further increasing the radius R, i.e., $R = 1.2\,\mathrm{cm}$ and $R = 1.8\,\mathrm{cm}$, the interaction between rods gradually becomes weak, so that it is not evident for the large-sized rod aggregate that magneto-electric couplings between rods can change promptly as the incidence direction varies. As a consequence, the nonreciprocity tends to shrink for the cases of an increasing R, as shown in Fig. 6(d).

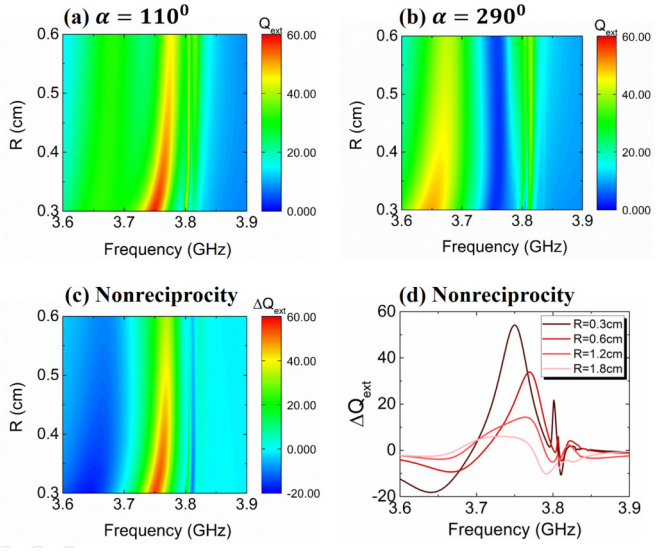

FIG. 6. The influence of the geometrical parameter, the array radius R, on the extinction efficiencies spectra at the incidence angles of (a) $\alpha = 110^\circ$ and (b) $\alpha = 290^\circ$. (c),(d) The corresponding variation of scattering nonreciprocity for opposite incidence in (a),(b). Four specified cases for different R are examined in (d), including the large-sized rod aggregates, i.e., $R = 1.2\,\mathrm{cm}$ and $R = 1.8\,\mathrm{cm}$.

IV. DISCUSSION AND CONCLUSION

We remark that the observed scattering nonreciprocity comes from the cooperative effect between the rods. However, it is essential to simultaneously break all related symmetries in the rod clusters, including time-reversal, spatial inversion, and rotational symmetries. Much previous work on linear and nonlinear nonreciprocal systems has shown that the condition of time-reversal symmetry breaking on the goal of nonreciprocity is requisite, and additionally an external bias (or self-biasing) as well as geometry asymmetry should be also employed or realized. More discussions on the interplay between broken spatiotemporal symmetries and scattering nonreciprocity are given in Fig. 7. For example, the subwavelength rod cluster, containing three different but nonmagnetic rods, is considered in Fig. 7(a). The preservation of time-reversal symmetries leads to the restoration of the scattering reciprocity, as shown in Fig. 7(b). Also, the extinction remains nearly unchanged in Fig. 7(d), once the spatial inversion and rotational symmetries of the structure are maintained with three identical gyromagnetic rods arranged in Fig. 7(c). Further details as well as more cases are given in the Appendix.

In summary, we study and analyze the unique nonreciprocal scattering phenomena by a set of finite number gyromagnetic cylindrical rods with deep-subwavelength size. Importantly, it is found that the asymmetrical magnetoelectric cross interaction between rods can effectively enable unidirectional nonreciprocal transparency: scattering is strong and enhanced for one incident direction, whereas nearly zero scattering occurs for the opposite incidence. Such results may help us understand the interplay between nonreciprocity and broken spatiotemporal symmetries and give us deep insight

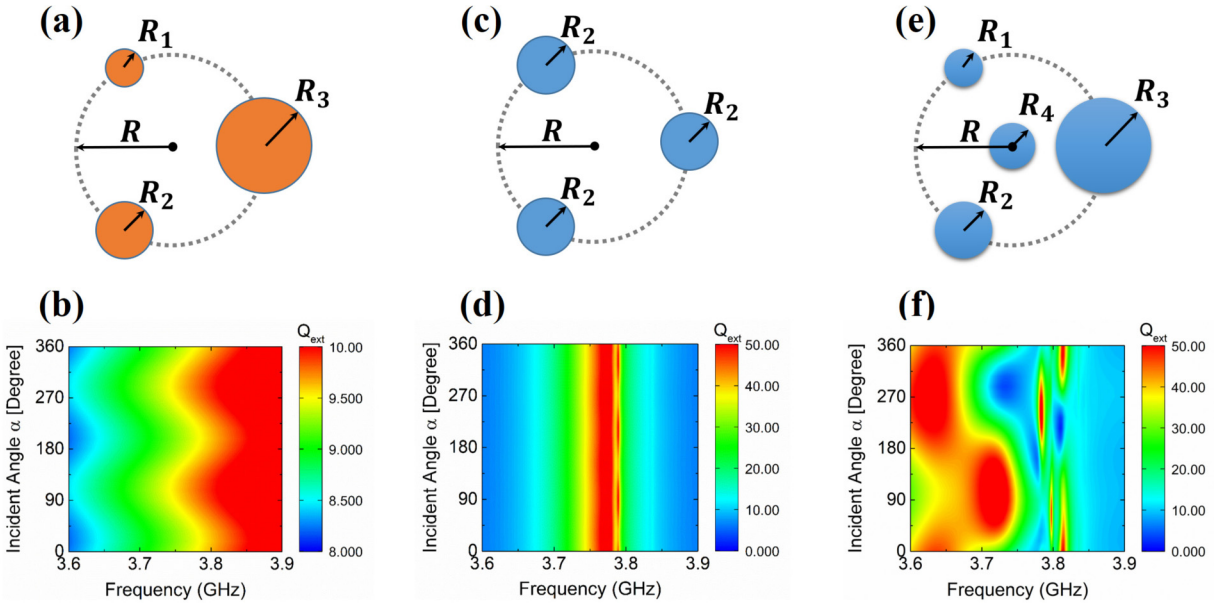

FIG. 7. Calculations on extinction efficiencies [(b), (d), (f)] contributed by all multipoles and all magneto-electric interactions for more cases: (a) three nonmagnetic rods, (c) three identical gyromagnetic rods, (e) four gyromagnetic rods. Here $R_1 = 0.08\,\text{cm}$, $R_2 = 0.12\,\text{cm}$, $R_3 = 0.20\,\text{cm}$, $R_4 = 0.096\,\text{cm}$, and $R = 0.4\,\text{cm}$. In the cases (c) and (e), the applied static magnetic field is the same as that in Fig. 2(a).

into the asymmetrical scattering problem in a variety of subwavelength rod clusters.

ACKNOWLEDGMENTS

This work was supported by the Natural Science Foundation of Jiangsu Province (Grant No. BK20181263), the Hong Kong Research Grants Council (Grants No. C6013-18G and No. AoE/P-502/20) and the National Natural Science Foundation of China (Grant No. 11774053, 12174052).

APPENDIX: INTERPLAY BETWEEN BROKEN SPATIOTEMPORAL SYMMETRIES AND SCATTERING NONRECIPROCITY

Several scattering configurations are demonstrated here to see the interplay between broken spatiotemporal symmetries and scattering nonreciprocity. Figure 7(b) shows the extinction efficiency for the trimer structure in Fig. 7(a), when the external static magnetic field is absent. Other geometrical parameters for individual rods remain unchanged compared to those in Fig. 2(a). The permeability elements in Eq. (1) are then changed to be $\mu_1 = 1$ and $\mu_2 = 0$. So the present structure in consideration just involves in the conventional nonmagnetic dielectric material, and preserves the time-reversal symmetry. In comparison with the extinction for the case of incident angle $\alpha \in [0^\circ, 180^\circ]$ and that of $\alpha \in [180^\circ, 360^\circ]$, it is observed in Fig. 7(b) that the scattering is restored to reciprocal. We also examine in Figs. 7(c) and 7(d) the effect of spatial symmetry in the structure on the scattering nonreciprocity. In Fig. 7(c), three identical rods are taken into account with the same radius $R_2 = 0.12\,\text{cm}$, in the presence of the same external magnetic field as that used in Fig. 2(a). It is clearly shown in Fig. 7(d) that the restoration of spatial inversion and rotational symmetries results in the nearly constant extinction at a frequency which is independent of the direction of incident waves. Finally, we consider another case for an aggregate containing more rods, i.e., four rods shown in Fig. 7(e), by inserting an additional rod with radius $R_4 = 0.096\,\text{cm}$ at the center of the circular array in Fig. 2(a). As expected, the simultaneous spatiotemporal breaking unambiguously gives rise to the pronounced scattering nonreciprocity indicated in Fig. 7(f). Moreover, compared to Fig. 5(a), the introduction of the fourth rod induces a bit of redshift at the frequency for the nonreciprocal transparency, and the possible enhancement of coupling between rods also allows it occur over the relatively broader frequency range.

[1] C. F. Bohren and D. R. Huffman, *Absorption and Scattering of Light by Small Particels* (John Wiley, New York, 2008).

[2] L. R. Hirsch, R. J. Stafford, J. A. Bankson, S. R. Sershen, B. Rivera, R. E. Price, J. D. Hazle, N. J. Halas, and J. L. West, Nanoshell-mediated near-infrared thermal therapy of tumors under magnetic resonance guidance, Proc. Natl. Acad. Sci. USA **100**, 13549 (2003).

[3] H. A. Atwater and A. Polman, Plasmonics for improved photovoltaic devices, Nat. Mater. **9**, 205 (2010).

[4] A. V. Kabashin, P. Evans, S. Pastkovsky, W. Hendren, G. A. Wurtz, R. Atkinson, R. Pollard, V. A. Podolskiy and A. V. Zayats, Plasmonic nanorod metamaterials for biosensing, Nat. Mater. **8**, 867 (2009).

[5] A. Alù and N. Engheta, Cloaking a Sensor, Phys. Rev. Lett. **102**, 233901 (2009).

[6] C. W. Hsu, B. G. Delacy, S. G. Johnson, J. D. Joannopoulos, and M. Soljačić, Theoretical criteria for scattering dark states in nanostructured particles, Nano Lett. **14**, 2783 (2014).

[7] R. Alaee, D. Lehr, R. Filter, F. Lederer, E.-B. Kley, C. Rockstuhl, and A. Tünnermann, Scattering dark states in multiresonant concentric plasmonic nanorings, ACS Photonics **2**, 1085 (2015).

[8] R. Alaee, A. Safari, V. Sandoghdar, and R. W. Boyd, Kerker effect, superscattering, and scattering dark states in atomic antennas, Phys. Rev. Research **2**, 043409 (2020).

[9] Z. Ruan and S. Fan, Superscattering of Light from Subwavelength Nanostructures, Phys. Rev. Lett. **105**, 013901 (2010).

[10] Z. Ruan and S. Fan, Design of subwavelength superscattering nanospheres, Appl. Phys. Lett. **98**, 043101 (2011).

[11] C. Qian, X. Lin, Y. Yang, X. Xiong, H. Wang, E. Li, I. Kaminer, B. Zhang, and H. Chen, Experimental Observation of Superscattering, Phys. Rev. Lett. **122**, 063901 (2019).

[12] A. Mirzaei, I. V. Shadrivov, A. E. Miroshnichenko, and Y. S. Kivshar, Superabsorption of light by multilayer nanowires, Nanoscale **7**, 17658 (2015).

[13] K. Ladutenko, P. Belov, O. P.-Rodríguez, A. Mirzaei, A. E. Miroshnichenko, and I. V. Shadrivov, Superabsorption of light by nanoparticles, Nanoscale **7**, 18897 (2015).

[14] B. H. Woo, I. C. Seo, E. Lee, S. Y. Kim, T. Y. Kim, S. C. Lim, H. Y. Jeong, C. K. Hwangbo, and Y. C. Jun, Dispersion control of excitonic thin films for tailored superabsorption in the visible region, ACS Photonics **4**, 1138 (2017).

[15] L. Cheng, R. Alaee, A. Safari, M. Karimi, L. Zhang, and R. W. Boyd, Superscattering, superabsorption, and nonreciprocity in nonlinear antennas, ACS Photonics **8**, 585 (2021).

[16] M. Kerker, D.-S. Wang, and C. L. Giles, Electromagnetic scattering by magnetic spheres, J. Opt. Soc. Am. **73**, 765 (1983).

[17] W. Liu, A. E. Miroshnichenko, D. N. Neshev, and Y. S. Kivshar, Broadband unidirectional scattering by magneto-electric core-shell nanoparticles, ACS Nano **6**, 5489 (2012).

[18] D. Pan, T. Feng, W. Zhang, and A. A. Potapov, Unidirectional light scattering by electric dipoles induced in plasmonic nanoparticles, Opt. Lett. **44**, 2943 (2019).

[19] A. V. Poshakinskiy and A. N. Poddubny, Optomechanical Kerker Effect, Phys. Rev. X **9**, 011008 (2019).

[20] H. K. Shamkhi, K. V. Baryshnikova, A. Sayanskiy, P. Kapitanova, P. D. Terekhov, P. Belov, A. Karabchevsky, A. B. Evlyukhin, Y. Kivshar, and A. S. Shalin, Transverse Scattering and Generalized Kerker Effects in All-Dielectric Mie-Resonant Metaoptics, Phys. Rev. Lett. **122**, 193905 (2019).

[21] Z. Lin, H. Ramezani, T. Eichelkraut, T. Kottos, H. Cao, and D. N. Christodoulides, Unidirectional Invisibility Induced by $\mathcal{PT}$-Symmetric Periodic Structures, Phys. Rev. Lett. **106**, 213901 (2011).

[22] L. Feng, Y.-L. Xu, W. S. Fegadolli, M.-H. Lu, J. E. B. Oliveira, V. R. Almeida, Y.-F. Chen, and A. Scherer, Experimental demonstration of a unidirectional reflectionless parity-time metamaterial at optical frequencies, Nat. Mater. **12**, 108 (2013).

[23] A. Regensburger, C. Bersch, M.-A. Miri, G. Onishchukov, D. N. Christodoulides, and U. Peschel, Parity-time synthetic photonic lattices, Nature (London) **488**, 167 (2012).

[24] Y. D. Chong, L. Ge, and A. D. Stone, PT-Symmetry Breaking and Laser-Absorber Modes in Optical Scattering Systems, Phys. Rev. Lett. **106**, 093902 (2011).

[25] X. Yin and X. Zhang, Unidirectional light propagation at exceptional points, Nat. Mater. **12**, 175 (2013).

[26] V. Achilleos, Y. Aurégan, and V. Pagneux, Scattering by Finite Periodic $\mathcal{PT}$-Symmetric Structures, Phys. Rev. Lett. **119**, 243904 (2017).

[27] H. Zhou, J. Y. Lee, S. Liu, and B. Zhen, Exceptional surfaces in PT-symmetric non-Hermitian photonic systems, Optica **6**, 190 (2019).

[28] V. A. Fedotov, P. L. Mladyonov, S. L. Prosvirnin, A. V. Rogacheva, Y. Chen, and N. I. Zheludev, Asymmetric Propagation of Electromagnetic Waves through a Planar Chiral Structure, Phys. Rev. Lett. **97**, 167401 (2006).

[29] P. Grahn, A. Shevchenko, and M. Kaivola, Theoretical description of bifacial optical nanomaterials, Opt. Express **21**, 23471 (2013).

[30] A. S. Schwanecke, V. A. Fedotov, V. V. Khardikov, S. L. Prosvirnin, Y. Chen, and N. I. Zheludev, Nanostructured metal film with asymmetric optical transmission, Nano. Lett. **8**, 2940 (2008).

[31] E. Plum, V. A. Fedotov, and N. I. Zheludev, Planar metamaterial with transmission and reflection that depend on the direction of incidence, Appl. Phys. Lett. **94**, 131901 (2009).

[32] C. Menzel, C. Helgert, C. Rockstuhl, E.-B. Kley, A. Tünnermann, T. Pertsch, and F. Lederer, Asymmetric Transmission of Linearly Polarized Light at Optical Metamaterials, Phys. Rev. Lett. **104**, 253902 (2010).

[33] D. L. Sounas and A. Alù, Extinction symmetry for reciprocal objects and its implication on cloaking and scattering manipulation, Opt. Lett. **39**, 4053 (2014).

[34] C. Caloz, A. Alù, S. Tretyakov, D. Sounas, K. Achouri, and Z.-L. Deck-Léger, Electromagnetic nonreciprocity, Phys. Rev. Appl. **10**, 047001 (2018).

[35] Y.-P. Wang, J. W. Rao, Y. Yang, P.-C. Xu, Y. S. Gui, B. M. Yao, J. Q. You, and C.-M. Hu, Nonreciprocity and Unidirectional Invisibility in Cavity Magnonics, Phys. Rev. Lett. **123**, 127202 (2019).

[36] K. M. Sliwa, M. Hatridge, A. Narla, S. Shankar, L. Frunzio, R. J. Schoelkopf, and M. H. Devoret, Reconfigurable Josephson Circulator/Directional Amplifier, Phys. Rev. X **5**, 041020 (2015).

[37] Z. Yu and S. Fan, Complete optical isolation created by indirect interband photonic transitions, Nat. Photonics **3**, 91 (2009).

[38] L. Bi, J. Hu, P. Jiang, D. H. Kim, G. F. Dionne, L. C. Kimerling, and C. A. Ross, On-chip optical isolation in monolithically integrated non-reciprocal optical resonators, Nat. Photonics **5**, 758 (2011).

[39] M. Shalaby, M. Peccianti, Y. Ozturk, and R. Morandotti, A magnetic nonreciprocal isolator for broadband terahertz operation, Nat. Commun. **4**, 1558 (2013).

[40] W. C. Wong, W. Wang, W. T. Yau, and K. H. Fung, Topological theory for perfect metasurface isolators, Phys. Rev. B **101**, 121405(R) (2020).

[41] J. Wang, H. Y. Dong, Q. Y. Shi, W. Wang, and K. H. Fung, Coalescence of nonreciprocal exceptional points in magnetized $\mathcal{PT}$-symmetric systems, Phys. Rev. B **97**, 014428 (2018).

[42] W. Wang, W. T. Yau, Y. Cui, J. Wang, and K. H. Fung, Maxwell's demon-like nonreciprocity by non-Hermitian gyrotropic metasurfaces, Phys. Rev. Research **3**, L022006 (2021).

[43] H. Lira, Z. Yu, S. Fan, and M. Lipson, Electrically Driven Nonreciprocity Induced by Interband Photonic Transition on a Silicon Chip, Phys. Rev. Lett. **109**, 033901 (2012).

[44] N. A. Estep, D. L. Sounas, J. Soric, and A. Alù, Magnetic-free nonreciprocity and isolation based on parametrically modulated coupled-resonator loops, Nat. Phys. **10**, 923 (2014).

[45] B. Peng, S. K. Özdemir, F. Lei, F. Monifi, M. Gianfreda, G. L. Long, S. Fan, F. Nori, C. M. Bender, and L. Yang, Parity-time-symmetric whispering-gallery microcavities, Nat. Phys. **10**, 394 (2014).

[46] L. Chang, X. Jiang, S. Hua, C. Yang, J. Wen, L. Jiang, G. Li, G. Wang, and M. Xiao, Parity-time symmetry and variable optical isolation in active-passive-coupled microresonators, Nat. Photonics **8**, 524 (2014).

[47] C. W. Ling, J. Wang, and K. H. Fung, Formation of nonreciprocal bands in magnetized diatomic plasmonic chains, Phys. Rev. B **92**, 165430 (2015).

[48] D. M. Pozar, *Microwave Engineering*, 2nd ed. (Wiley, New York, 1998).

[49] J. Jin, S. Liu, Z. Lin, and S. T. Chui, Effective-medium theory for anisotropic magnetic metamaterials, Phys. Rev. B **80**, 115101 (2009).

[50] J. Wang, K. F. Lee, H. Y. Dong, Z.-G. Dong, S. F. Yu, and K. H. Fung, Collective resonances in a circular array of gyromagnetic rods, Phys. Rev. B **101**, 045425 (2020).

[51] D. Felbacq, G. Tayeb, and D. Maystre, Scattering by a random set of parallel cylinders, J. Opt. Soc. Am. A **11**, 2526 (1994).

[52] W. Liu and A. E. Miroshnichenko, Scattering invisibility with free-space field enhancement of all-dielectric nanoparticles, Laser Photonics Rev. **11**, 1700103 (2017).

[53] W. Liu, Generalized Magnetic Mirrors, Phys. Rev. Lett. **119**, 123902 (2017).

[54] M. Abramovitz and I. A. Stegun, *Handbook of Mathematical Functions* (Dover, New York, 1970).